ATLAS NOTE

ATLAS-CONF-2014-037

July 3, 2014

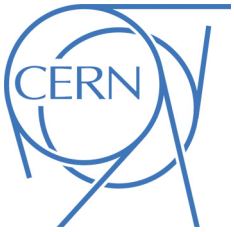

Limits on metastable gluinos from ATLAS SUSY searches at 8 TeV

The ATLAS Collaboration

Abstract

In some models of supersymmetry, the gluino is metastable and travels a measurable distance in the detector before decaying to quarks (or a gluon) and a neutralino. Results of ATLAS SUSY searches designed for promptly decaying squarks and gluinos, produced at 8 TeV pp collisions at the Large Hadron Collider, are reinterpreted in the context of metastable gluinos. Limits are presented as a function of gluino mass, gluino lifetime, and neutralino mass. Decays of the gluino to $t\bar{t}\tilde{\chi}_1^0$ are studied separately from decays to $q\bar{q}\tilde{\chi}_1^0$ (where q is a non-top quark) or $g\tilde{\chi}_1^0$. The gluino is excluded at 95% confidence level up to $m_{\tilde{g}} = 850\,(900)$ GeV for decays to $q\bar{q}\tilde{\chi}_1^0$/ $g\tilde{\chi}_1^0$ ($t\bar{t}\tilde{\chi}_1^0$), for a lifetime of 1 ns and $m_{\tilde{\chi}_1^0} = 100$ GeV.

ATLAS-CONF-2014-037
04 July 2014

1 Introduction

Gluinos ($\tilde{g}$) would be strongly produced with large cross sections and thus could be observable up to large masses at the LHC. ATLAS has excluded gluinos up to a mass of 1350 GeV, assuming prompt decays of the gluino to jets and missing transverse momentum ($E_{\mathrm{T}}^{\mathrm{miss}}$) [1]. For very long-lived gluinos, ATLAS and CMS have excluded charged gluino *R*-hadrons that escape the detector before decaying with a mass less than 1300 GeV [2, 3] and those that stop in the detector and then decay with a mass less than 830 GeV [4]. However, no limits on metastable gluinos decaying in flight inside the detector are available up to now since such a scenario was not explicitly considered.

Several compelling models of SUSY predict a metastable gluino. The observed value of the Higgs boson mass indicates squark masses around 10^3–10^5 TeV for small values of tanβ, a moderately fine-tuned scenario known as *mini-split* SUSY [5]. For these squark masses, a 1 TeV gluino could be metastable and decay within the detector with a visible decay length, as shown in figure 1.

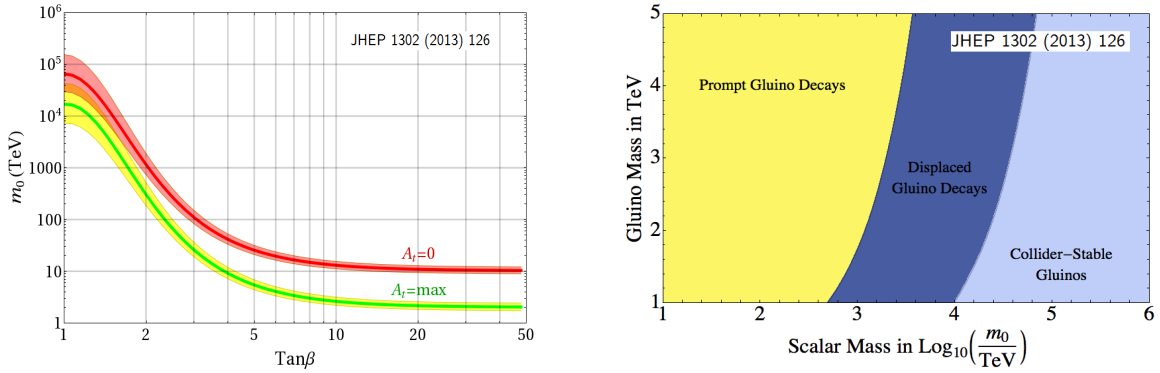

Figure 1: Left: The preferred scalar SUSY mass to have a Higgs boson mass consistent with observation, as a function of tanβ, for large and small top mixing (A_t). Right: Region of displaced gluino decays (metastable gluinos) as a function of scalar SUSY mass vs. gluino mass. The figures are taken from ref. [5].

Though designed to look for promptly decaying SUSY particles, various ATLAS searches can also be sensitive to metastable gluino decays. For instance, searches using high energy jets and large $E_{\mathrm{T}}^{\mathrm{miss}}$ could observe a signal from metastable gluino decays before the calorimeters. Searches using jets containing *b*-quarks (referred to as *b*-jets) and $E_{\mathrm{T}}^{\mathrm{miss}}$ can identify displaced jets from metastable gluino decays as *b*-jets. The sensitivity of these analyses to metastable gluinos depends on the reconstruction algorithms and analysis selections as well as the expected interactions of the gluino decay products with the detector.

This note presents the first re-interpretation of ATLAS SUSY searches in the context of metastable gluinos. The metastable gluino signals are fully simulated, including the hadronization of the colored $\tilde{g}$ into a colorless *R*-hadron, its possible interactions with the detector, and its decay. The signal simulation is further described in section 2. Two decay types, shown in figure 2, are considered separately:

- $\tilde{g}\to t\bar{t}\tilde{\chi}_1^0$, which would be the dominant decay if the top squark were the lightest squark; and
- $\tilde{g}\to q\bar{q}\tilde{\chi}_1^0$ (where q is a non-top quark: u,d,s,c,b), which is predicted for a mass-degenerate squark flavor scenario, or $\tilde{g}\to g\tilde{\chi}_1^0$. The model assumes equal branching ratios of the two decays, $q\bar{q}\tilde{\chi}_1^0$ or $g\tilde{\chi}_1^0$.

The following searches are considered, which use 20.3 fb^{-1} of pp collisions at $\sqrt{s}$ = 8 TeV recorded in 2012:

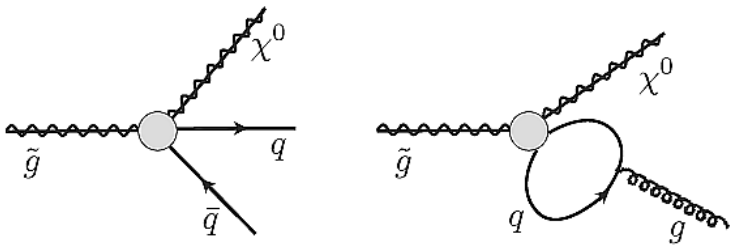

Figure 2: Diagrams for the decays of a long-lived gluino in split SUSY, from ref. [6]. The blob represents the four-point vertex generated after integrating out the heavy squark. The diagram on the left is a tree-level three-body decay to two quarks and a neutralino, while the diagram on the right is the loop-level two-body decay to a neutralino and a gluon. In certain regions of parameter space, the loop-induced decay can become dominant over the three-body decay [7].

- "7-10 jets": the event selection is based on 7,8,9,or ≥10 jets, $E_{\mathrm{T}}^{\mathrm{miss}}$, and 0,1, or >=2 b-tagged jets [8]
- "2-6 jets": the event selection is based on 2,3,4,5,or ≥6 jets and $E_{\mathrm{T}}^{\mathrm{miss}}$ [1]

Both searches look for new particles in final states with significant hadronic activity, $E_{\mathrm{T}}^{\mathrm{miss}}$, and no isolated electrons or muons.

2 Simulation

The simulated metastable gluino samples have gluino masses in the range 400–1400 GeV and neutralino masses in the range 20–1300 GeV. The gluino lifetime is varied from 1 ps–10 ns in general and up to 5 μs for some cases. The Pythia program [9], version 6.427, with CTEQ6L1 parton distribution functions (PDF) [10], is used to simulate pair production of gluinos. The cross sections are calculated to next-to-leading order in the strong coupling constant α_{S}, including the resummation of soft gluon emission at next-to-leading-logarithmic accuracy (NLO+NLL) [11, 12, 13, 14, 15].

The string hadronization model [16], incorporating specialized hadronization routines [17] for R-hadrons, is used to produce final states containing two R-hadrons. The ratio of singly-charged to neutral R-hadrons depends slightly on the gluino mass. In this analysis it is set close to unity, following LHC standards for R-hadron searches. The analysis sensitivity is assumed not to depend on the initial R-hadron charge. The simulation of R-hadron interactions with matter is handled by a special detector response simulation [18, 19] using Geant4 [20, 21] routines based on the *generic* [18, 22] scattering and spectrum model.

The gluinos within R-hadrons decay via the radiative process, $\tilde{g}\to g\tilde{\chi}_1^0$, or via $\tilde{g}\to q\bar{q}\tilde{\chi}_1^0$(decays involving top quarks are studied separately). These R-hadron decays are also simulated with Pythia, after being propagated in Geant4. Similarly, any bottom or charm hadrons resulting from the R-hadron decays are also decayed using Pythia, after being propagated in Geant4. The final simulated events then proceed through the standard ATLAS digitization simulation [21], which includes a realistic modeling of pileup pp interactions as observed during the 2012 data period, followed by event reconstruction.

3 Results

The results of the two searches are re-interpreted in the context of the metastable gluino models. The signal region definitions, background yields and their systematic uncertainties, statistical treatment, and

exclusion limit extraction methods used for these interpretations are those documented in refs. [1] and [8]. For the signal models, the yields are extracted by running these analysis selections. The sources of systematic uncertainties as well as the procedures used to extract them are the same as described in the corresponding references. Additional systematic uncertainties that may originate from reconstructing displaced objects are not considered in this study. The dominant sources of systematic uncertainty on the signal generally arise from the jet energy scale and resolution uncertainties. The b-tagging efficiency uncertainties dominate in signal regions where more than one b-jet is required, since the b-tagging efficiency for non-b (and non-c) jets has large uncertainties.

The achieved 95% confidence level (CL) exclusion limits are shown in figures 3-5 for the gluino decays to $q\bar{q}\tilde{\chi}_1^0$/ $g\tilde{\chi}_1^0$ and in figures 6-8 for the gluino decays to $t\bar{t}\tilde{\chi}_1^0$. For both gluino decay modes studied, we show limits on the $\tilde{\chi}^0$ mass for $m_{\tilde{g}}$= 800 GeV (near the sensitivity limit for heavy $\tilde{\chi}^0$) and limits on the $\tilde{g}$ mass for $m_{\tilde{\chi}^0}$=100 GeV and a "compressed" spectrum with the $\tilde{\chi}^0$ mass close to the $\tilde{g}$ mass (minus the mass of the gluino decay products), as a function of gluino lifetime. The expected exclusion limits are shown for the "7-10 jets" analysis and the "2-6 jets" analysis separately, together with the expected and observed combined results. The best expected limit at each point in parameter space is used for the combination of the two searches. The black points indicate the parameters of the simulated samples used to draw the limit curves.

Limits are only displayed within the boundary of the simulated points in parameter space (black dots on limit figures) and interpolated between those points; sensitivity is still expected for lower $\tilde{g}$ or $\tilde{\chi}^0$ mass and in many cases for longer or shorter lifetimes than was simulated. The "7-10 jets" search has no sensitivity to the gluino decays to $q\bar{q}\tilde{\chi}_1^0$/ $g\tilde{\chi}_1^0$ as this model leads to a relatively small jet multiplicity compared to the jet multiplicity requirements of that search. Both searches have good sensitivity in the gluino decays to $t\bar{t}\tilde{\chi}_1^0$ where they are are complementary. An example event display is shown in figure 9.

The sensitivity decreases for long lifetimes. Studying the effect of the analyses selections (tables 1-2) for various samples that only differ in the gluino lifetime, we observe that:

- The jet multiplicity decreases for lifetimes longer than 1 ns, as gluino decays often occur within or outside the calorimeter.

- In models with decays giving leptons (such as the gluino decays to $t\bar{t}\tilde{\chi}_1^0$) fewer events fail the lepton veto as the lifetime increases since leptons significantly displaced from the primary vertex are not identified.

- The standard object and event cleaning decrease the signal acceptance as the lifetime increases. The largest acceptance drop comes from a selection on the "charged fraction" (f_{ch}), defined as the ratio of the scalar sum of the p_{T} of the tracks associated to the jet and divided by the jet p_{T}, and on the "electromagnetic energy fraction" (f_{EM}), defined as the fractional energy measured in the electromagnatic layer of the calorimeter. The two leading jets with $p_{\text{T}} > 100$ GeV and $|\eta| < 2.0$ are required to have $f_{\text{ch}} > 0.02$, or $f_{\text{ch}} > 0.05$ and $f_{\text{EM}} > 0.9$; the event is otherwise rejected. This selection is very effective at rejecting cosmic and beam background events. Other event cleaning cuts are defined in reference [23], with the "Looser" selection being used. It should also be noted that the p_{T} of the jets selected in the analyses is large enough to not necessitate explicit additional requirements on them originating from the primary vertex, so no efficiency is lost due to such a requirement for displaced jets.

- Signal regions that require b-jets have enhanced acceptance for small gluino lifetimes that are comparable with the b-quark lifetimes, as jets are more often reconstructed as b-jets, as shown in figure 10.

4 Conclusion

We have studied the sensitivity to metastable gluinos of several ATLAS searches for strongly produced SUSY particles and their combination, as a function of gluino mass, gluino lifetime, and neutralino mass. The gluino is excluded up to $m_{\tilde{g}} = 850$ (900) GeV for decays to $q\bar{q}\tilde{\chi}_1^0$/ $g\tilde{\chi}_1^0$ ($t\bar{t}\tilde{\chi}_1^0$), for a lifetime of 1 ns and $m_{\tilde{\chi}_1^0} = 100$ GeV.

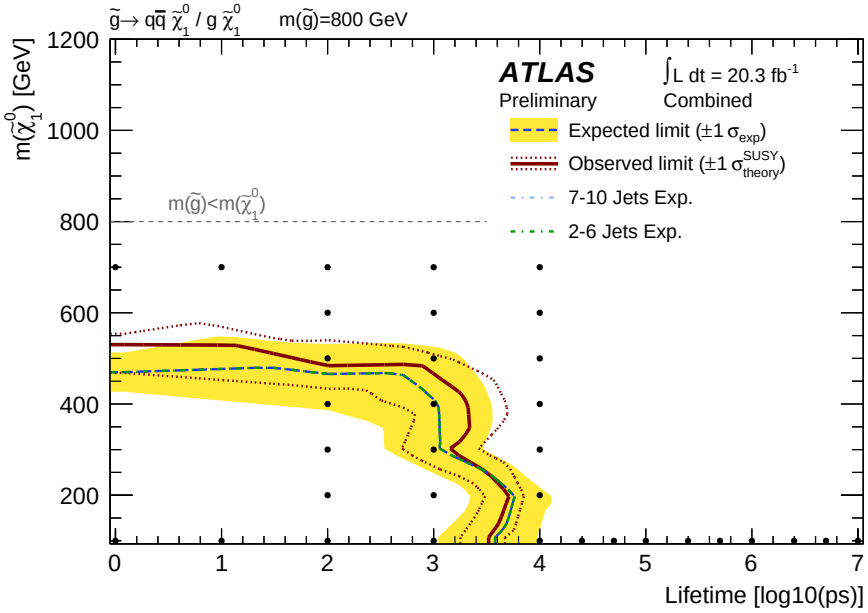

Figure 3: 95% CL excluded $\tilde{\chi}_1^0$ mass as a function of $\tilde{g}$ lifetime, for $m_{\tilde{g}} = 800$ GeV and $\tilde{g}\to q\bar{q}\tilde{\chi}_1^0$/ $g\tilde{\chi}_1^0$ decays.

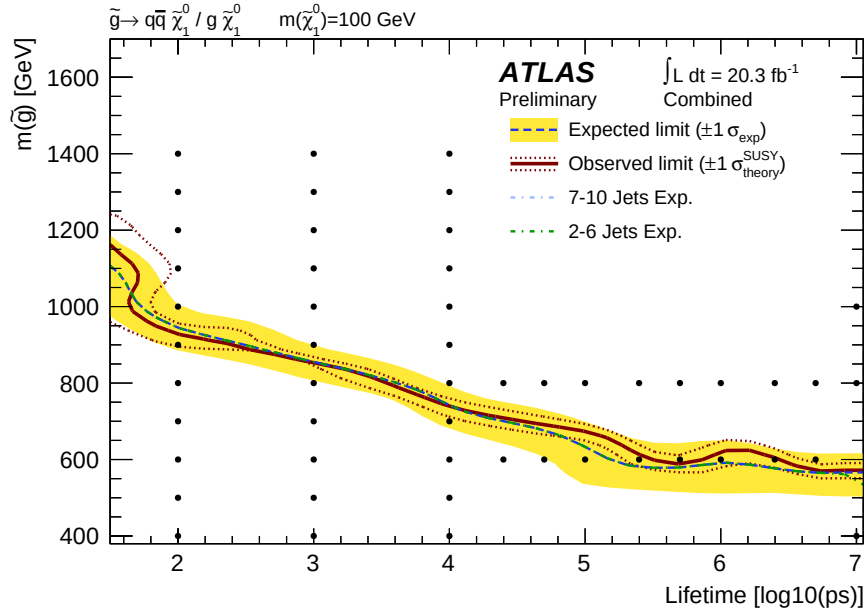

Figure 4: 95% CL excluded $\tilde{g}$ mass as a function of $\tilde{g}$ lifetime, for $m_{\tilde{\chi}_1^0} = 100$ GeV and $\tilde{g}\to q\bar{q}\tilde{\chi}_1^0$/ $g\tilde{\chi}_1^0$ decays.

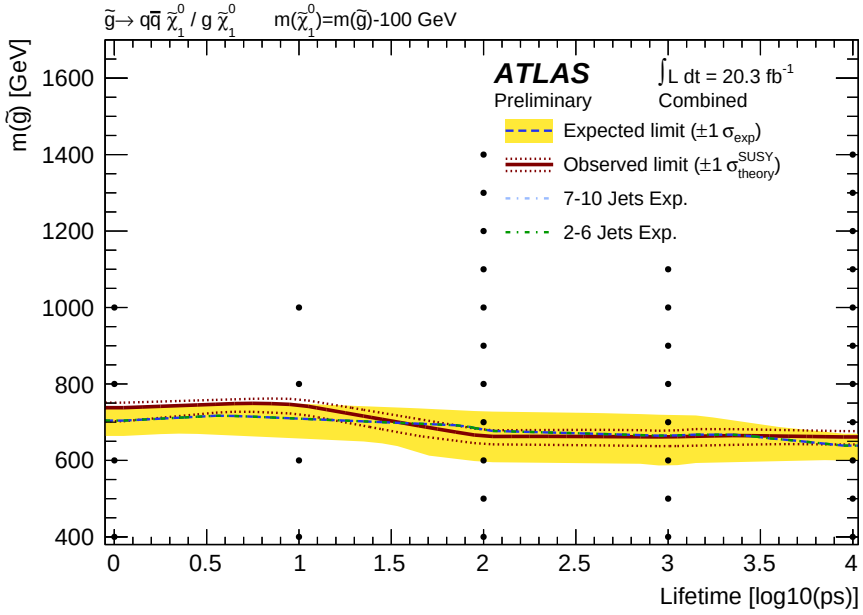

Figure 5: 95% CL excluded $\tilde{g}$ mass as a function of $\tilde{g}$ lifetime, for $m_{\tilde{\chi}_1^0} = m_{\tilde{g}} - 100$ GeV and $\tilde{g}\to q\bar{q}\tilde{\chi}_1^0$/ $g\tilde{\chi}_1^0$ decays. Samples were not simulated for lifetimes longer than 10 ns for this compressed scenario, as the small mass gap can only affect events with decays before or within the calorimeters. Sensitivity for these longer lifetimes is shown in figure 4.

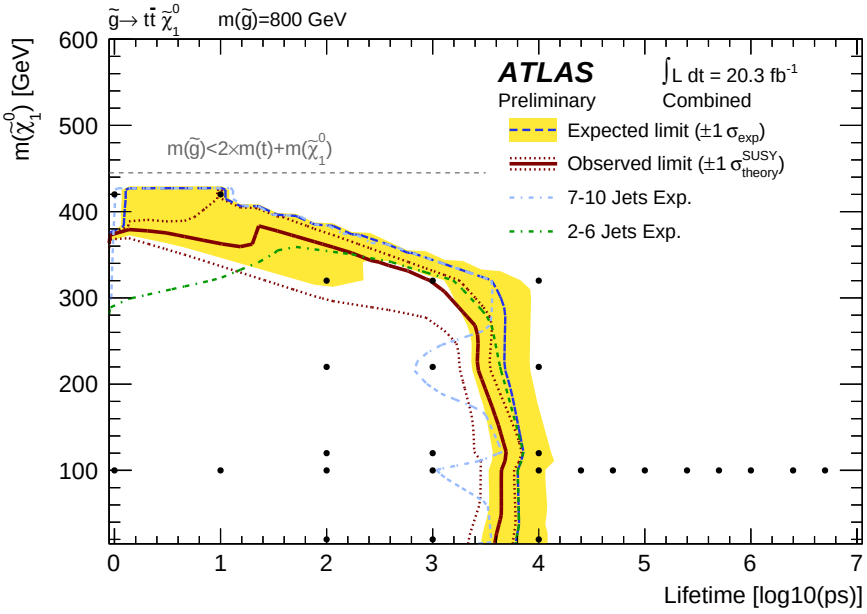

Figure 6: 95% CL excluded $\tilde{\chi}_1^0$ mass as a function of $\tilde{g}$ lifetime, for $m_{\tilde{g}} = 800$ GeV and $\tilde{g}\to t\bar{t}\tilde{\chi}_1^0$ decays. At low lifetimes, the "7-10 jet" analysis has sensitivity beyond the "2-6 jets" analysis due to the use of b-tagging information.

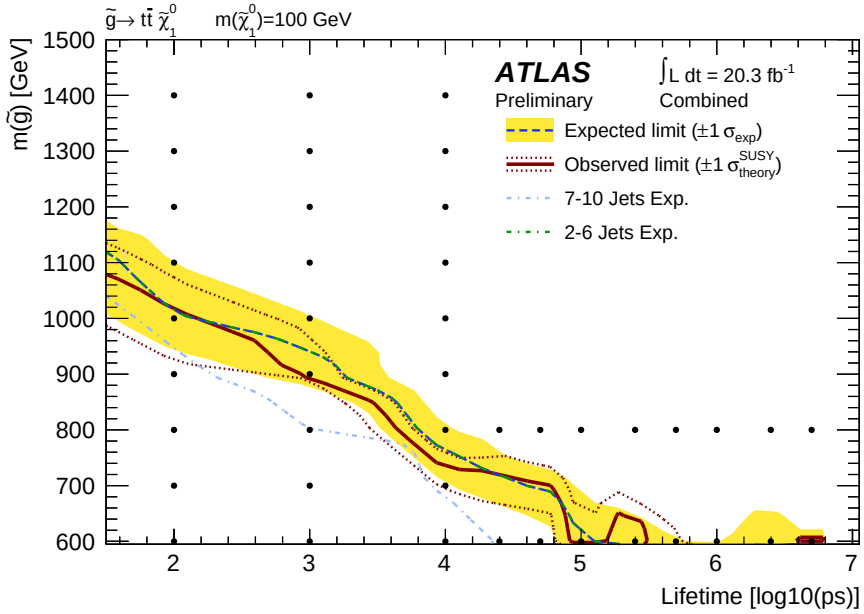

Figure 7: 95% CL excluded $\tilde{g}$ mass as a function of $\tilde{g}$ lifetime, for $m_{\tilde{\chi}_1^0} = 100$ GeV and $\tilde{g}\to t\bar{t}\tilde{\chi}_1^0$ decays.

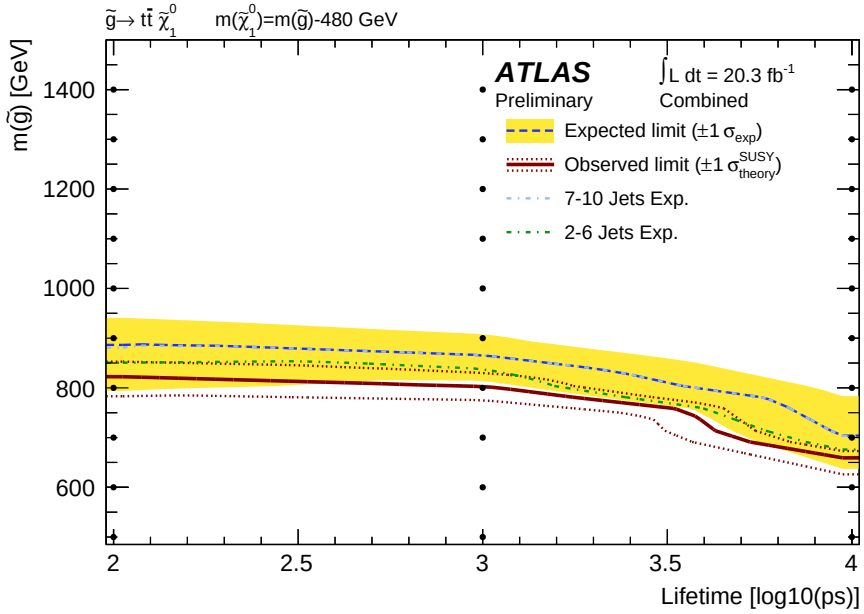

Figure 8: 95% CL excluded $\tilde{g}$ mass as a function of $\tilde{g}$ lifetime, for $m_{\tilde{\chi}_1^0} = m_{\tilde{g}} - 480$ GeV and $\tilde{g}\to t\bar{t}\tilde{\chi}_1^0$ decays. The mass difference of 480 GeV leaves a mass gap of ≈100 GeV, similar to the other decay case, after accounting for the masses of the two hadronized top quarks. Samples were not simulated for lifetimes longer than 10 ns for this compressed scenario, as the small mass gap can only affect events with decays before or within the calorimeters. Sensitivity for these longer lifetimes is shown in figure 7. Samples were also not simulated for lifetimes less than 100 ps, but sensitivity does extend to these lower lifetimes, as seen in figure 6.

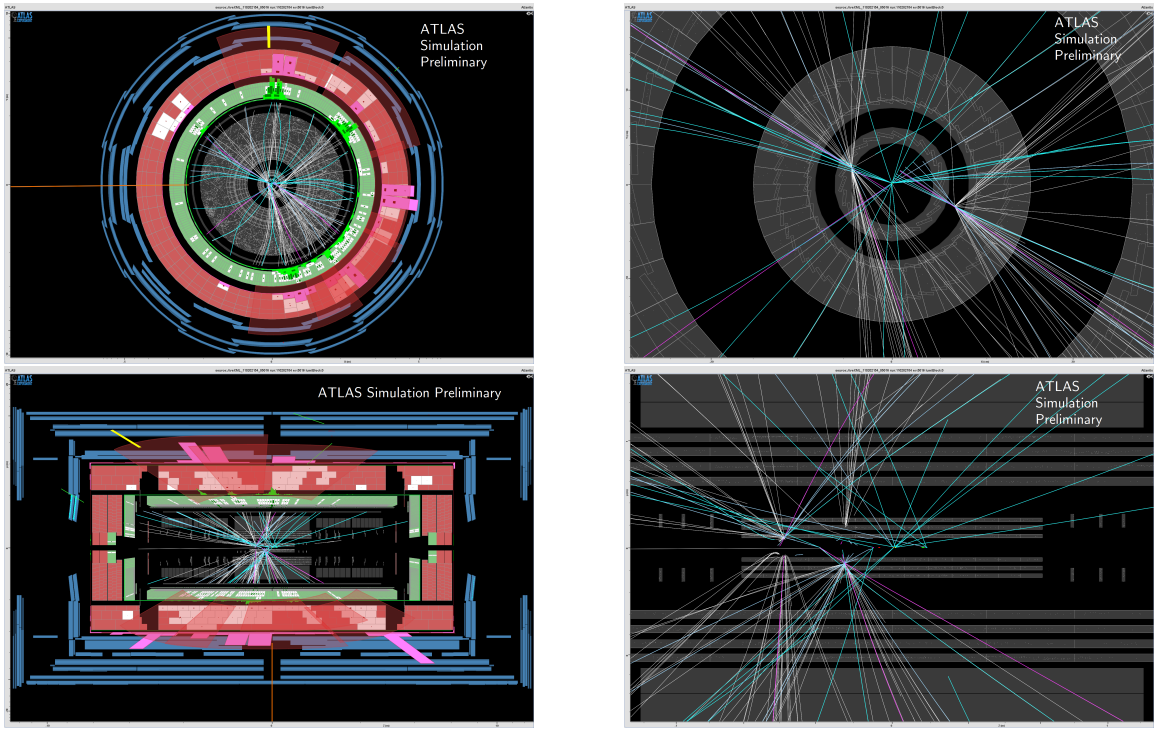

Figure 9: Displays of a simulated event with 600 GeV gluinos with 1 ns lifetime decaying to $t\bar{t}\tilde{\chi}^0$ with a 100 GeV $\tilde{\chi}^0$. Colored tracks are reconstructed, and white tracks are simulated charged tracks with p_{T} above 1 GeV.

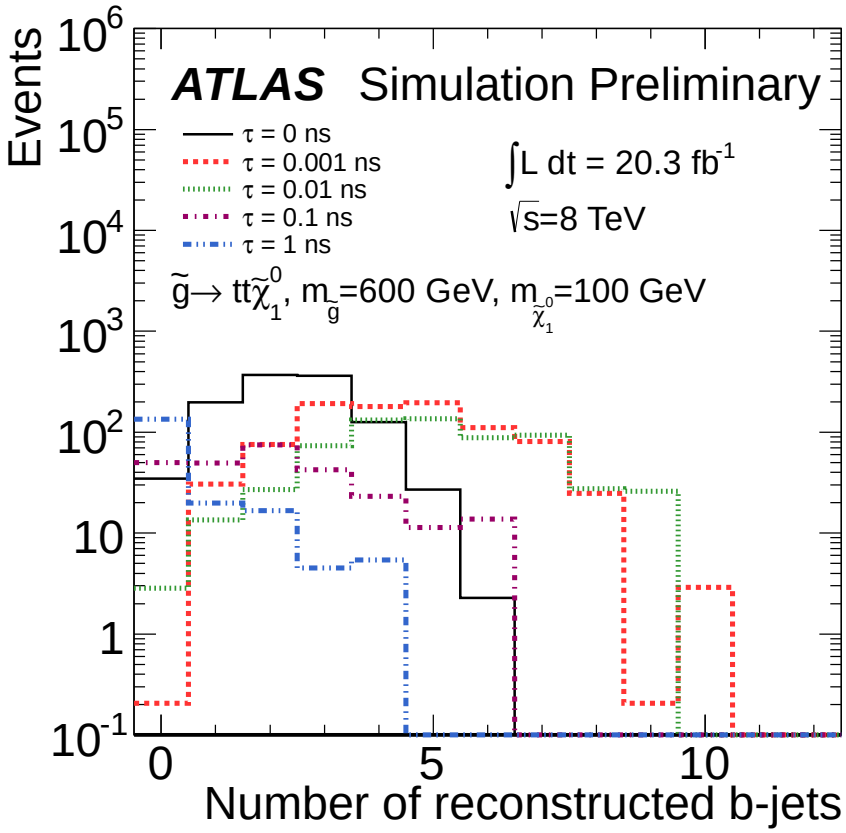

Figure 10: b-jet multiplicity for events passing the "7-10 jets" analysis (flavour-stream) preselection, with gluino to $t\bar{t}\tilde{\chi}_1^0$ decays, a gluino of mass 600 GeV, and a $\tilde{\chi}^0$of mass 100 GeV, for various gluino lifetimes. The samples corresponding to 10^{-12} s and 10^{-11} s have very similar behavior: the gluino lifetime is comparable to the b-quark lifetime (10^{-12} s), therefore most jets are reconstructed as b-jets. The prompt gluino decay sample shows much smaller b-jet multiplicity, as expected.

	0.001 ns	0.01 ns	0.1 ns	1 ns	10 ns	Expected	Observed
Trigger (6 jets with $E_T > 45$ GeV)	16200	15700	15800	14700	5200		
Primary vertex and event cleaning	15400	13000	13000	13800	4700		
Lepton Veto	8300	8100	10700	13200	4600		
Further event cleaning	8100	5500	2000	1800	1100		
8j50, $\|\eta\| < 2.0$	1100	700	260	180	50		
& $E_T^{miss}/\sqrt{H_T} > 4.0$ GeV$^{1/2}$	700	420	190	120	36		
& 0 bjet	$0.200 \pm 0.200 \pm 0.003$	$2.8 \pm 2.8 \pm 2.8$	$38 \pm 10^{+12}_{-1}$	$87 \pm 16 \pm 24$	$31 \pm 6^{+4}_{-5}$	35 ± 4	40
& 1 bjet	$28 \pm 10^{+9}_{-16}$	$14 \pm 7^{+8}_{-3}$	$41 \pm 12^{+7}_{-11}$	$16 \pm 7^{+11}_{-7}$	$3.9 \pm 2.8^{+5.8}_{-1.2}$	40 ± 10	44
& $\geq$ 2 bjets	$2305 \pm 176^{+3093}_{-1455}$	$1770 \pm 165^{+2752}_{-1152}$	$269 \pm 45^{+204}_{-128}$	$30 \pm 14^{+25}_{-16}$	$5.9 \pm 5.9^{+7.3}_{-3.6}$	50 ± 10	44
9j50, $\|\eta\| < 2.0$	310	260	80	70	20		
& $E_T^{miss}/\sqrt{H_T} > 4.0$ GeV$^{1/2}$	190	130	49	39	15		
& 0 bjet	$0.0^{+2.6}_{-0.0}$	$0.0^{+2.6}_{-0.0}$	$5.1 \pm 3.6^{+8.9}_{-3.8}$	$26 \pm 9^{+32}_{-26}$	$14 \pm 4^{+5}_{-4}$	3.3 ± 0.7	5
& 1 bjet	$11 \pm 6 \pm 6$	$2.7 \pm 2.7 \pm 2.7$	$11 \pm 6 \pm 4$	$6.2 \pm 4.4^{+6.5}_{-5.8}$	$0.0^{+2.6}_{-0.0}$	6.1 ± 1.7	8
& $\geq$ 2 bjets	$691 \pm 97^{+959}_{-472}$	$618 \pm 105^{+1055}_{-458}$	$90 \pm 29^{+81}_{-48}$	$13 \pm 8 \pm 10$	$0.0^{+2.6}_{-0.0}$	8.0 ± 2.7	7
$\geq$ 10j50, $\|\eta\| < 2.0$	140	110	44	36	0.0		
& $E_T^{miss}/\sqrt{H_T} > 4.0$ GeV$^{1/2}$	$53 \pm 12^{+11}_{-9}$	$67 \pm 14^{+13}_{-17}$	$28 \pm 9 \pm 4$	$26 \pm 9 \pm 4$	$0.0^{+2.6}_{-0.0}$	1.37 ± 0.35	3
7j80, $\|\eta\| < 2.0$	210	150	70	48	13		
& $E_T^{miss}/\sqrt{H_T} > 4.0$ GeV$^{1/2}$	130	80	50	33	8.8		
& 0 bjet	$0.0^{+2.6}_{-0.0}$	$0.0^{+2.6}_{-0.0}$	$14 \pm 6^{+2}_{-0}$	$22 \pm 8^{+3}_{-6}$	$6.9 \pm 3.1^{+2.8}_{-3.2}$	11.0 ± 2.2	12
& 1 bjet	$7.1 \pm 5.1^{+4.7}_{-7.1}$	$2.7 \pm 2.7^{+3.8}_{-2.7}$	$13 \pm 7 \pm 2$	$0.0^{+2.6}_{-0.0}$	$1.9 \pm 1.9 \pm 1.9$	17 ± 6	17
& $\geq$ 2 bjets	$460 \pm 75^{+599}_{-319}$	$323 \pm 68^{+493}_{-203}$	$49 \pm 17^{+29}_{-22}$	$19 \pm 10 \pm 9$	$0.0^{+2.6}_{-0.0}$	25 ± 10	13
$\geq$ 8j80, $\|\eta\| < 2.0$	48	50	25	14	1.1		
& $E_T^{miss}/\sqrt{H_T} > 4.0$ GeV$^{1/2}$	25	27	22	8.7	0.0		
& 0 bjet	$0.0^{+2.6}_{-0.0}$	$0.0^{+2.6}_{-0.0}$	$1.90 \pm 1.90 \pm 0.03$	$8.3 \pm 4.8^{+3.9}_{-2.8}$	$0.0^{+2.6}_{-0.0}$	0.9 ± 0.6	2
& 1 bjet	$3.7 \pm 3.7^{+0.7}_{-3.7}$	$0.0^{+2.6}_{-0.0}$	$7.6 \pm 5.4^{+3.8}_{-4.2}$	$0.0^{+2.6}_{-0.0}$	$0.0^{+2.6}_{-0.0}$	1.5 ± 0.9	1
& $\geq$ 2 bjets	$91 \pm 37^{+152}_{-62}$	$145 \pm 54^{+293}_{-107}$	$29 \pm 13^{+20}_{-16}$	$0.0^{+2.6}_{-0.0}$	$0.0^{+2.6}_{-0.0}$	3.3 ± 2.2	3

Table 1: Cut-flow of the "7-10 jets" search for a $\tilde{g}\rightarrow t\bar{t}\tilde{\chi}_1^0$ model, where the gluinos have mass of 600 GeV and the $\tilde{\chi}_1^0$ has a mass of 100 GeV, for five different gluino lifetimes. The numbers are normalized to the luminosity, 20.3 fb^{-1}, taking into account that the cross section for a gluino of 600 GeV is 1.3 pb. The % uncertainties correspond to the statistical (first number) and experimental (second number) ones. 10000 events are generated per sample, except for the 10 ns samples, for which 20000 events were generated. The b-jet requirements are made separately, as in the signal region definitions. The "Looser" event cleaning, as well as a cosmic muon veto, are applied under the 'event cleaning' selection. Further selections such as the f_{ch} and f_{EM} selection on the two leading jets > 100 GeV and $|\eta|$ <2.0 (described in the text) and others correcting for problematic detector regions are applied under the 'further event cleaning' selection.

	0.001 ns	0.01 ns	0.1 ns	1 ns	10 ns	Expected	Observed
Normalized n. events	26700	26700	26700	26700	26700		
Primary vertex	26300	26300	26300	26500	21600		
Event cleaning	26000	25800	25900	26100	20600		
0 Lepton	25500	25600	25600	26000	20400		
$E_{\mathrm{T}}^{\mathrm{miss}} > 160$ GeV	19700	19700	19700	19300	12200		
& $E_{\mathrm{T}}^{\mathrm{miss}} / \sqrt{H_{\mathrm{T}}} > 8$ GeV$^{1/2}$	14600	14500	14700	13800	7900		
SR2jl	10110 ±110 ±160	10600 ±110 ±140	10380 ±110 ±140	9300 ±110 ±140	3860 ±110 ±140	13000 ± 1000	12315
SR2jm	1110 ±27 ±13	1100 ±27 ±23	1060 ±27 ±10	780 ±27 ±23	390 ±27 ±23	760±50	715
SR2j	180 ±11 ±14	180 ±11 ±14	185 ±10 ±37	86 ±11 ±10	75 ±11 ±10	125±10	133
SR3j	21 ±2 ±2	23 ±2 ±2	15 ±2 ±2	10 ±2 ±2	5 ±2 ±2	5 ± 1	7
SR4jl-	3400 ±25 ±22	3800 ±25 ±24	3600 ±25 ±18	3100 ±25 ±22	1070 ±25 ±22	2120 ± 110	2169
SR4jl	2080 ±46 ±110	2300 ±46 ±180	2200 ±50 ±120	1640 ±46 ±110	540 ±46 ±110	630±50	608
SR4jm	135 ±5 ±4	160 ±5 ±4	140 ±5 ±4	110 ±5 ±4	47 ±5 ±4	37 ±6	24
SR4jt	18 ±1 ±1	19 ±1 ±1	10 ±1 ±1	10 ±1 ±1	5 ±1 ±1	3 ± 1	0
SR5j	610 ±10 ±4	710 ±10 ±9	550 ±10 ±9	490 ±11 ±10	170 ±11 ±9	126 ± 13	121
SR6jl	347 ±11 ±14	397 ±10 ±14	310 ±10 ±15	300 ±11 ±15	98 ±11 ±13	110 ±11	121
SR6jm	214 ±6 ±7	250 ±6 ±8	190 ±6 ±8	150 ±6 ±8	55 ±6 ±25	33 ± 6	39
SR6jt	54 ±2 ±1	65 ±2 ±2	50 ±2 ±2	32 ±2 ±1	17 ±2 ±2	5 ± 1	5
SR6jt+	57 ±2 ±2	64 ±2 ±5	60 ±2 ±2	28 ±2 ±2	12 ±2 ±2	5 ± 2	6

Table 2: Cut-flow of the "2-6 jets" search for the $\tilde{g}\rightarrow q\bar{q}\tilde{\chi}_1^0$ / $g\tilde{\chi}_1^0$ model. Other details are as in table 1.

References

[1] ATLAS Collaboration, arXiv:1405.7875 [hep-ex].

[2] ATLAS Collaboration, Phys.Lett. **B720** (2013) 277–308, arXiv:1211.1597 [hep-ex].

[3] CMS Collaboration, JHEP **1307** (2013) 122, arXiv:1305.0491 [hep-ex].

[4] ATLAS Collaboration, Phys.Rev. **D88** (2013) 112003, arXiv:1310.6584 [hep-ex].

[5] A. Arvanitaki, N. Craig, S. Dimopoulos, and G. Villadoro, JHEP **1302** (2013) 126, arXiv:1210.0555 [hep-ph].

[6] P. W. Graham, K. Howe, S. Rajendran, and D. Stolarski, Phys. Rev. D **86** (2012) 034020.

[7] P. Gambino, G. Giudice, and P. Slavich, Nuclear Physics B **726** no. 12, (2005) 35 – 52.

[8] ATLAS Collaboration, JHEP **1310** (2013) 130, arXiv:1308.1841 [hep-ex].

[9] T. Sjostrand, S. Mrenna, and P. Skands, JHEP **05** (2006) 026, arXiv:hep-ph/0603175.

[10] J. Pumplin, D. Stump, J. Huston, H. Lai, P. M. Nadolsky, et al., JHEP **0207** (2002) 012, arXiv:hep-ph/0201195.

[11] W. Beenakker, R. Hopker, M. Spira, and P. Zerwas, Nucl.Phys. **B492** (1997) 51–103, arXiv:hep-ph/9610490 [hep-ph].

[12] A. Kulesza and L. Motyka, Phys.Rev.Lett. **102** (2009) 111802, arXiv:0807.2405 [hep-ph].

[13] A. Kulesza and L. Motyka, Phys.Rev. **D80** (2009) 095004, arXiv:0905.4749 [hep-ph].

[14] W. Beenakker, S. Brensing, M. Kramer, A. Kulesza, E. Laenen, et al., JHEP **0912** (2009) 041, arXiv:0909.4418 [hep-ph].

[15] W. Beenakker, S. Brensing, M. Kramer, A. Kulesza, E. Laenen, et al., Int.J.Mod.Phys. **A26** (2011) 2637–2664, arXiv:1105.1110 [hep-ph].

[16] B. Andersson, G. Gustafson, G. Ingelman, and T. Sjostrand, Phys. Rept. **97** (1983) 31–145.

[17] M. Fairbairn et al., Phys. Rept. **438** (2007) 1–63, arXiv:hep-ph/0611040.

[18] A. C. Kraan, Eur. Phys. J. **C37** (2004) 91–104, arXiv:hep-ex/0404001.

[19] R. Mackeprang and D. Milstead, Eur. Phys. J. **C66** (2010) 493–501, arXiv:hep-ph/0908.1868.

[20] GEANT4 Collaboration, Nucl. Instrum. Meth. **A506** (2003) 250–303.

[21] ATLAS Collaboration, Eur. Phys. J. **C70** (2010) 823–874, arXiv:hep-ex/1005.4568v1.

[22] R. Mackeprang and A. Rizzi, Eur. Phys. J. **C50** (2007) 353–362, arXiv:hep-ph/0612161.

[23] ATLAS Collaboration, Tech. Rep. ATLAS-CONF-2012-020, CERN, Geneva, Mar, 2012.